Positive streamer in a weak field in air: A moving avalanche-to-streamer transition

A. A. Kulikovsky*
Research Computing Center, Moscow State University, 119899 Moscow, Russia
(Received 18 December 1997)

Two-dimensional (2D) simulation of a positive streamer in air between a point anode and a plane cathode is performed within the scope of a diffusion-drift model. A fine structure of streamer head is obtained. Based on the simulation results, the head is treated as a moving region of an avalanche-to-streamer transition (AST). Using ''empirical'' relations, which follow from 2D simulations, and applying the Meek's concept of an AST, two simple analytical models of streamer dynamics in a weak field are offered. The *isolated head model* gives results which correspond well to that of 2D simulations. The *potential model* qualitatively explains an effect recently detected in experiment of streamer expansion in a weak external field. Both models allow one to calculate the streamer velocity, number density of electrons, and radius of the plasma channel from a single input parameter. [S1063-651X(98)02406-4]

PACS number(s): 52.80.Mg, 52.80.Tn

I. INTRODUCTION

The first phase of electric breakdown in atmospheric pressure gases is that thin and bright plasma channels (streamers) are formed and rapidly bridge overvolted electrodes. A positive streamer moves towards the cathode, against the direction of electron drift. If an anode is sharpened, a high field is concentrated near the tip. A streamer is created near the anode, leaves the high-field region, and moves in a low external field due to its own space charge field.

The physics of positive streamer propagation in gases is of fundamental interest since Rogowski [1] discovered the effect of streamer breakdown. The ability of a positive streamer to propagate in a weak external field makes streamer corona discharge an attractive instrument for plasma chemical applications [2]. Hereafter ''weak'' denotes a field well below the field of static breakdown ($\simeq 30$ kV cm^{-1} in atmospheric air).

A crucial role in streamer dynamics is played by the streamer head, where a high field due to the separation of charges is created. The streamer velocity usually varies in the range 10^7–10^8 cm s^{-1}; the radius of the head is about 10^{-1}–10^{-2} cm. This combination makes difficult direct experimental observation of the head.

It is known now that streamer propagation in a weak external field is supported by electron drift, collisional ionization in the head, and photoionization of the gas ahead of it. The problem is essentially nonlinear and this puts numerical modeling in the forefront.

During the past decade two-dimensional (2D) simulations of streamers in a uniform field [3–9] provided clear and sharp visual pictures of the effect of streamer breakdown and gave properties of streamers in strong (above static breakdown) fields. In the majority of these works the streamer was described by hydrodynamic equations for charged particles coupled by Poisson's equation for an electric field. Kunhardt and Tzeng [5] were the first to perform 2D Monte Carlo calculations of the avalanche-to-streamer transition in a self-consistent field. However, the kinetic model is extremely time consuming and in [5] only the initial stage of streamer growth was simulated.

Guo and Wu [6] have taken into account the momentum and energy balance of electrons in the streamer problem. Their model gave results close to those from the diffusion-drift model, which have been used in [3,4,7–9]. Within the scope of this model electrons are considered as massless particles in local equilibrium with the electric field.

A so-called 1.5-dimensional model [10] operates with one-dimensional (1D) continuity equations for the densities of charged particles along with an approximate or accurate 2D description of the electric field. This model has been widely used in various modifications for simulation of streamers in a weak field [11–15]. This model, however, requires one to prescribe the channel radius and distribution of space charge. In [16] a variable streamer radius was incorporated into the 1.5D model using an approximate analytical description of the field and electron density.

In Sec. III it will be shown that the distribution of space charge at the tip is more essential for an accurate description of streamer advancement. This information can be deduced only from fully 2D models. Because of multiple computational difficulties, there still is a lack of accurate and reliable fully 2D numerical simulations of positive streamers in a weak field. The gradient of the electron density in the head is $\partial \ln n_e/\partial z \simeq 2\times 10^3$ cm^{-1} and the velocity of electron drift is $\simeq 3\times 10^7$ cm s^{-1}. This combination makes the problem time consuming. A simple analytical theory of streamer dynamics is very desirable.

The first analytical model of streamer dynamics in a weak field was offered by Dawson and Winn [17]. They treated the proliferation of the streamer channel as a process of drift, ionization growth, and diffusion expansion of an equivalent avalanche, which moves in the field of the head. A similar model, based on the energy balance of the moving avalanche, was developed by Gallimberti [18].

Another approach was offered by Dyakonov and Kachorovskii [19]. Following the early work of Loeb [20] they assumed that streamer propagation occurs due to the creation of an ionization domain (ID) at the streamer tip. The exis-

*Electronic address: akul@oberon.phys.msu.su

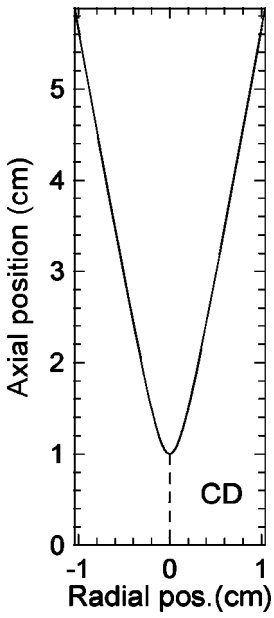

FIG. 1. The electrodes and computational domain (CD). The anode (curve) is a hyperboloid of revolution $(z/b)^2-(r/a)^2=1$, where $a=0.18$ cm, $b=1$ cm. The radius of curvature of the tip is $a^2/b=0.0324$ cm. The cathode is at $z=0$.

tence of this domain was confirmed in 2D simulations by Wang and Kunhardt [21]. According to [19], in this region, ionization growth of the plasma density occurs while the Maxwellian relaxation time in a newborn plasma is much less than the ionization time. When these times become comparable, ionization growth is halted. This gives simple relations between streamer parameters. Similar arguments were used recently in [22]. This approach does not involve avalanche drift and diffusion: the plasma channel elongates due to ionization multiplication of charges in the ID.

All these theories (except Loeb's) imply that the streamer channel is charged uniformly or use some arbitrary space charge distribution. The results of 2D simulations in a strong external field [9] have shown, however, that the head of the streamer has a fine structure. The space charge is concentrated in a thin layer around the plasma channel, as has been predicted by Loeb. The characteristic space scale of streamer growth in a strong field is the width of the space charge layer. The latter is almost one order of magnitude less than the radius of channel.

In this paper results of 2D simulations of streamer propagation in air in a weak field between a point anode and a plane cathode are reported. The model and results of the simulation are described in Sec. II. The detailed structure of the streamer head is presented and the role of various processes is examined. Based on the simulation results, two simple analytical models of the streamer are offered (Sec. III) and the physics of streamer propagation is discussed (Sec. IV).

II. TWO-DIMENSIONAL SIMULATION

A. Model

Consider a hyperboloid anode 1 cm over a plane cathode in air (Fig. 1). The origin of cylindrical system of coordinates (r,z) is placed at the cathode surface opposite the anode tip. Axis z is directed towards the anode.

Streamer dynamics is governed by the following system of equations:

$$\frac{\partial n_e}{\partial t}+\frac{1}{r}\frac{\partial (r j_{er})}{\partial r}+\frac{\partial j_{ez}}{\partial z}=S_{\rm ph}+S_i-S_{\rm att}-L_{ep}, \qquad (1)$$

$$\frac{\partial n_p}{\partial t}=S_{\rm ph}+S_i-L_{ep}-L_{pn}, \qquad (2)$$

$$\frac{\partial n_n}{\partial t}=S_{\rm att}-L_{pn}, \qquad (3)$$

$$\Delta V=-\frac{e}{\varepsilon_0}(n_p-n_e-n_n). \qquad (4)$$

Here

$$\mathbf{j}_e=-D_e\nabla n_e-\mu_e n_e\mathbf{E}, \quad \mathbf{E}=-\nabla V,$$

is the electron current density with the components $\{j_{er},j_{ez}\}$, n the number density, D and μ the diffusion coefficient and mobility, respectively, $\mathbf{E}$ the strength, and V the potential of the electric field. The subscripts e, p, and n refer to electrons, positive ions, and negative ions, respectively; e in Eq. (4) is the absolute value of electron charge.

In Eqs. (1)–(3), S and L stand for sources and losses of charged particles. $S_{\rm ph}$ is the rate of charged particle generation due to photoionization in a gas volume, S_i the rate of collisional ionization, $S_{\rm att}$ the rate of electron attachment, L_{ep} the rate of electron-ion recombination, and L_{pn} the rate of ion-ion recombination.

The rate of collisional ionization was calculated with the usual local field relation $S_i=\mu_e E\alpha n_e$. The Townsend ionization coefficient α in air was calculated as [23]

$$\alpha=AN\exp\left(-\frac{E_*}{E}\right). \qquad (5)$$

Here N is the number density of gas molecules, $E_*=BN$, and A and B are constants taken to be $A=1.4\times10^{-16}$ cm^2 and $B=660$ Td [23] (1 Td $\equiv10^{-17}$ V cm^2).

The relation (5) describes well experimental data in the range $10<E/N<150$ Td. The simulation shows that at the tip E/N can reach $\simeq$800 Td. For $E/N>150$ Td experimental data [24] are available, but they require a more sophisticated fit. The α plays a central role in analytical models (Sec. III) and to simplify things we have used the relation (5) for all values of E/N.

Two-body dissociative attachment and three-body attachment of electrons to oxygen molecules were taken into account. Electron mobility, the diffusion coefficient, and reactions between charged particles were taken in accordance with recommendations of [23]. Transport coefficients and reaction rates used in the calculations are listed in [9].

The rate of photoionization was calculated within the scope of the model [25]. In N_2:O_2 mixtures the radiation of excited nitrogen photoionizes oxygen molecules. The model of [25] is based on the assumption that the major contribution to the rate of photoionization gives radiation in the spec-

tral range 980–1025 Å, where one can neglect the absorption of radiation by nitrogen. Here 1025 Å is the photoionization threshold of O_2. Below 980 Å the radiation is strongly absorbed by nitrogen and gives a minor contribution to photoelectron production. Taking into account the fine structure of the oxygen absorption spectrum, in [25] the integral over the wavelength domain 980–1025 Å in the general expression for the rate of photoionization was calculated. Geometrical details specific to the streamer problem were considered in [8]. Here the emission of radiation from the entire volume of the streamer channel has been accounted for [relation (B2) in [8]].

The system of equations (1)–(4) was converted to a finite-difference form with the method of control volume. The fluxes of electrons were calculated with the more accurate Scharfetter-Gummel algorithm [26]. Poisson's equation was solved by the symmetrical successive overrelaxation method.

The computational grid contained $N_r \times N_z = 134 \times 640$ nodes and had the following structure. In the radial direction the region $0 < r < 0.15$ cm was covered by a nonuniform fine grid and then the cells were expanded exponentially up to $r \simeq 1.1$ cm. In the axial direction 200 uniform cells formed the base coarse grid. To resolve accurately the steep gradients the streamer head was covered by a window of uniform fine grid ($\simeq 400$ cells), which was moved along with the head. The dimensions of the smallest cell were $h_r \times h_z = 0.0008 \times 0.000\,63$ cm. Details of the numerical procedure are presented in [26,8].

A small plasma spot was placed at the anode tip to initiate streamer formation. The number densities of seed electrons and ions were of Gaussian shape in the radial and axial directions:

$$n_p(r,z)|_{t=0} = n_e(r,z)|_{t=0} = n_0 \exp\left[-\left(\frac{r}{\sigma_r}\right)^2 - \left(\frac{z-z_0}{\sigma_z}\right)^2 \right], \tag{6}$$

where $z_0 = d - \sigma_z$, $\sigma_r = 0.01$ cm, and $\sigma_z = 0.025$ cm. For immediate initiation of the streamer $n_0 = 10^{14}$ cm^{-3} was taken. Initially there were no negative ions in the gap: $n_n|_{t=0} = 0$.

B. Numerical results

The results presented below were obtained for the following conditions: the gas is dry air (N_2:O_2 = 80:20) under a pressure of 760 Torr and a temperature of 300 K. The applied voltage $V_0 = 13$ kV. Figure 2 shows the contour lines of the electron density and absolute value of the electric field. The evolution of axial profiles of the electron density and electric field is shown in Fig. 3. Figure 4 displays the variation of the streamer velocity in the gap along with the variation of the peak field at the tip of the streamer, $E_{\max}$.

Two phases can clearly be distinguished. The first one lasts $\simeq 5$ ns. During this time interval the radius of the plasma channel increases (Fig. 2). The streamer velocity decreases along with $E_{\max}$ (Fig. 4). To the end of this phase $E_{\max}$ reduces by half and the streamer channel has the shape of a cone. Similar behavior of the streamer velocity near the anode was detected in experiments [27]. A strong correlation between the velocity and $E_{\max}$ shows that the rapid streamer deacceleration near the anode is related to the fall of the peak field.

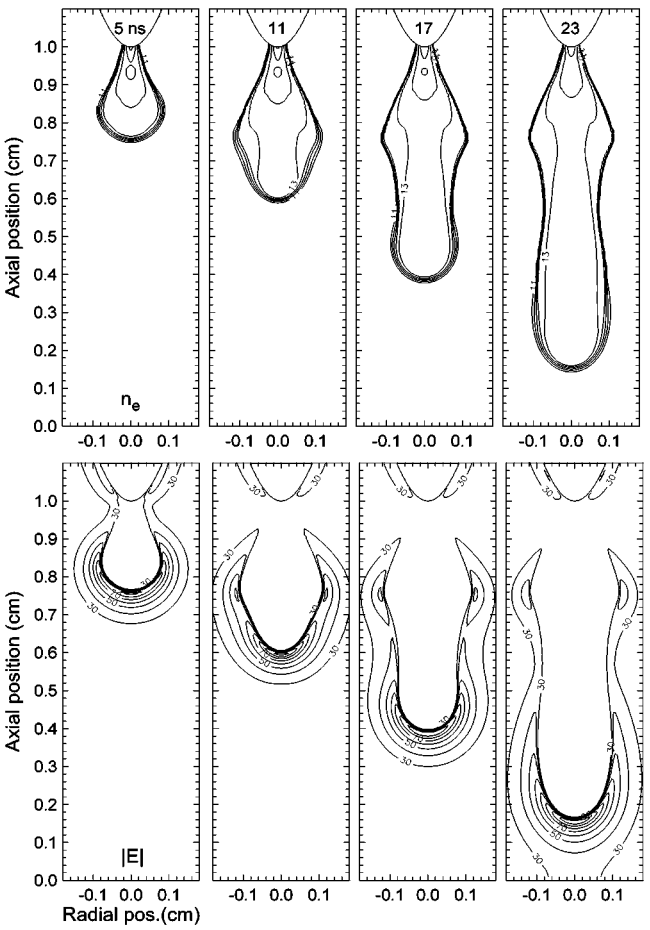

FIG. 2. Contour lines of the electron number density (upper row) and absolute value of the electric field (lower row). Time moments are 5, 11, 17, and 23 ns. Shown are n_e contours $10^{11}, 10^{11.5}, 10^{12} \ldots$ cm^{-3}. The outermost contour is 10^{11} cm^{-3}. Electric field contours are 30,40, ... kV cm^{-1}.

In the second phase (5–20 ns) the streamer propagates in a low (15–5 kV cm^{-1}) Laplacian field with an almost constant radius of the plasma channel and $E_{\max}$ [Figs. 2 and 3(b)]. The velocity also practically does not change: this is a phase of stationary propagation.

To clarify the role of the various processes in the streamer dynamics, it is advisable to compare the terms in the electron continuity equation (1). The axial profiles of these terms at the moment 17 ns are presented in Fig. 5. As is seen, ahead of the streamer tip recombinaton and attachment are not essential and collisional ionization (S_i) dominates. Seed electrons are provided by the photoionization ($S_{\rm ph}$).

Figure 6 shows the leading terms in the electron continuity equation (1) in linear scale. It is seen that the characteristic width of the rate of ionization and the space charge curve are much the same. This fact is essential for further analysis. The two-dimensional shape of the rate of ionization (Fig. 7) confirms that the width l_ρ of the space charge layer around the streamer head defines the space scale of the region of plasma growth. The contour of S_i represents the ionization domain (Fig. 7).

The divergence of the electron current density is 2–3 times less than S_i and to a first approximation one can ne-

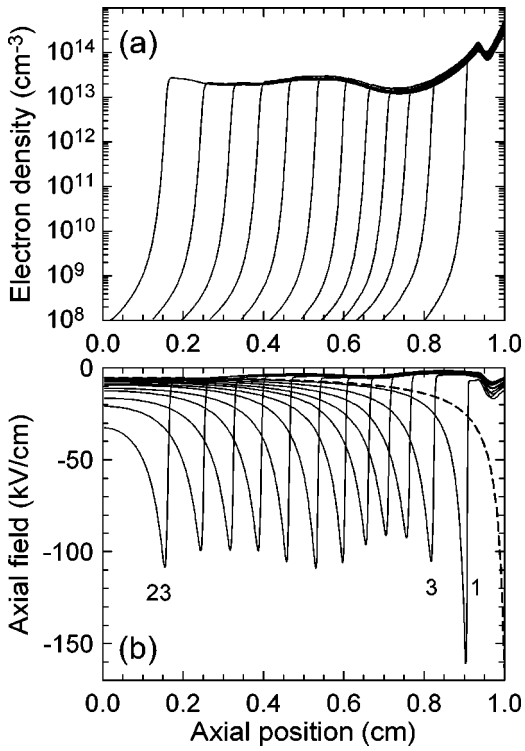

FIG. 3. Axial profiles of the electron density (a) and electric field (b). Time moments 1–23 ns, step 2 ns. The dotted curve in (b) shows the Laplacian field. The streamer propagates towards $z=0$.

glect this term in the balance of electrons ahead of the tip. However, this term is essential in the balance of space charge. It is the $\nabla \cdot \mathbf{j}_e$ which provides advancement of the space charge peak towards the cathode. The continuity equation for the space charge $\rho \equiv n_p - n_e - n_n$ follows from Eqs. (1)–(3),

$$\frac{\partial \rho}{\partial t} = \nabla \cdot \mathbf{j}_e , \tag{7}$$

and shows that the space charge is altered only by $\nabla \cdot \mathbf{j}_e$. Figure 6 clearly shows this: to the left of the space charge peak $\nabla \cdot \mathbf{j}_e > 0$, and thus the space charge grows at the new position. To the right of the peak $\nabla \cdot \mathbf{j}_e < 0$ and the space charge in the newly created segment of the streamer channel is removed.

III. ANALYTICAL MODELS OF A STREAMER IN A WEAK FIELD

A. ''Empirical'' relations and Meek's criterium

In [9] it has been shown that in a strong uniform external field, the peak value $E_{\max}$ of field at the streamer tip can be approximated as

$$E_{\max} = E_L + E_{\rho\,\max} = E_L + \frac{e}{\varepsilon_0}\frac{\rho_{\max} l_\rho}{3}, \tag{8}$$

where E_L is the Laplacian field, $E_{\rho\,\max}$ is the peak value of the field produced by the space charge, l_ρ the width of the space charge layer, and $\rho_{\max}$ the peak value of the space charge at the tip. The $E_{\max}$ calculated with $\rho_{\max}$ and l_ρ from

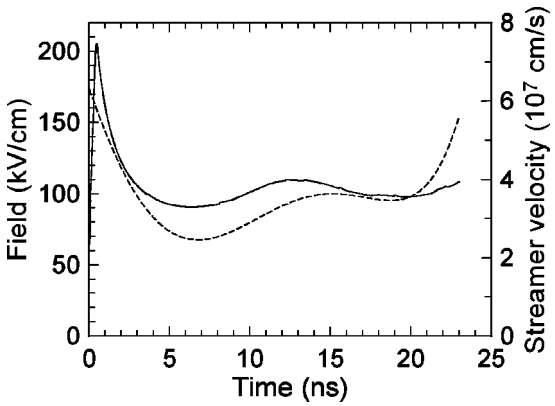

FIG. 4. The evolution of the peak value of the electric field (solid curve) and streamer velocity (dashed curve).

2D simulations is shown in Fig. 8. As is seen, the relation (8) describes the simulated $E_{\max}$ within an accuracy $\simeq 20\%$. Physically this means that the 2D distribution of space charge around the streamer head creates a peak field which coincides with the field at the surface of the uniformly charged ball. The radius of this equivalent ball is l_ρ and the space charge density inside it is $\rho_{\max}$.

However, outside this ball the field does not decrease as the inverse square of distance. Figure 9 shows the axial profiles of the space charge field. For further calculations an analytical fit of this curve is required. A reasonable approximation gives the combination of linear growth inside the space charge layer and a falloff, which is inversely proportional to the distance:

$$E_\rho(x) = \begin{cases} E_{\rho\,\max}\left(1 + \dfrac{x}{l_\rho}\right), & -l_\rho \leqslant x < 0, \\ E_{\rho\,\max} \Big/ \left(1 + \dfrac{x}{2l_\rho}\right), & x \geqslant 0. \end{cases} \tag{9}$$

Hereinafter $x = z_{\max} - z$ is counted from the position of the peak field $z_{\max}$ (Fig. 9). This fit was found to provide a good approximation of $E_\rho(x)$ under various voltages and anode geometries.

Relation (9) shows that if one moves away from the streamer tip towards the cathode, near the tip the field decreases as a field of a charged disk of radius $\simeq l_\rho$. Physically, this behavior is reasonable: the 2D distribution of space charge has a peak at the tip with the characteristic width of the order of l_ρ along the radial direction.

The results of 2D simulations allow one to calculate the ionization integral

$$M = \int_{-l_\rho}^{l_\rho} \alpha dx, \tag{10}$$

where the integration performs over the ionization domain. The dependence of M on the position of the streamer tip is shown in Fig. 10. In the middle of the gap ($0.35 < z_{\max} < 0.8$ cm) M varies in the range 18–22. This value is close to the well-known Meek's criterium of an avalanche-to-streamer transition (AST) in a uniform field [28]:

$$\alpha d = M_0 , \tag{11}$$

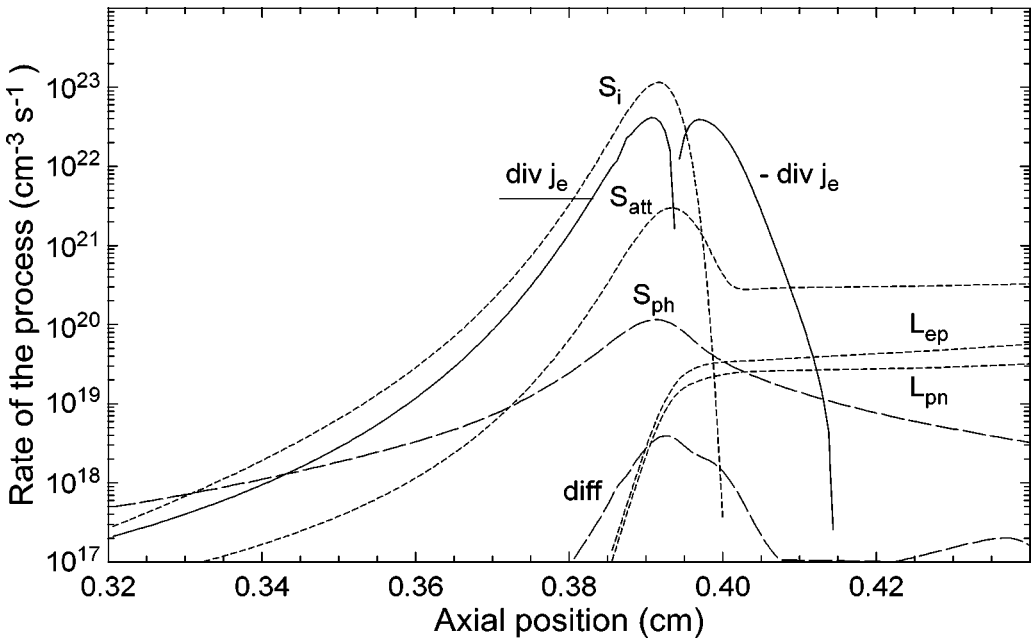

FIG. 5. Streamer head: the rates of the processes at the moment 17 ns. The designations are those used in Eq. (1). Dashed curves are the rates of collisional ionization S_i, photoionization $S_{\rm ph}$, attachment $S_{\rm att}$, electron-ion recombination L_{ep}, positive-negative ion recombination L_{pn}, and ''diff'' the diffusion part of $\nabla\cdot\mathbf{j}_e$, that is, $\nabla\cdot(D_e\nabla n_e)$. Solid curves: the term $\nabla\cdot\mathbf{j}_e$. All the rates are given in $\mathrm{cm}^{-3}\,\mathrm{s}^{-1}$.

where $M_0\simeq 18$–20. This suggests that the head of the streamer can be considered as the moving region of the AST. This analogy allows one to construct a simple model of the streamer.

Following Meek, the number of charges in the avalanche at the AST moment is

$$N_{\rho 0}=\exp(M_0)\simeq 10^8, \tag{12}$$

and hence it is reasonable to assume that the number of charges in the equivalent ball at the tip is

$$\frac{4}{3}\pi l_\rho^3\rho_{\max}=\exp(M). \tag{13}$$

From Eqs. (8) and (13) it follows that

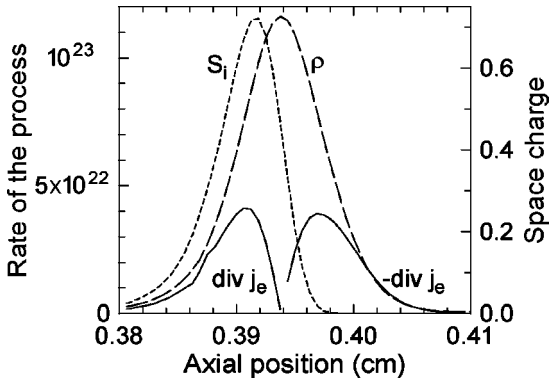

FIG. 6. Streamer head: the rates of the dominating processes at the moment 17 ns (linear scale) and the space charge. Dashed curves are S_i, the rate of collisional ionization; ρ, the space charge. Solid curves: the term $\nabla\cdot\mathbf{j}_e$ in Eq. (1). The rates are given in $\mathrm{cm}^{-3}\,\mathrm{s}^{-1}$; space charge is in $10^{13}\ \mathrm{cm}^{-3}$.

$$E_{\rho\max}=E_{\max}-E_L=\frac{e}{\varepsilon_0}\frac{\exp(M)}{4\pi l_\rho^2}. \tag{14}$$

The value of α rapidly decreases with the field and this allows one to extend the integration in Eq. (10) to infinity:

$$\int_{-l_\rho}^{\infty}\alpha dx=M. \tag{15}$$

In a weak field $E_L\ll E_{\max}$, and hence in the ionization domain $E(x)\simeq E_\rho(x)$. Substituting Eq. (5) with $E=E_\rho$ into Eq. (15) and using fit (9) one obtains the equation

$$\exp(-F)-F\,\mathrm{Ei}(1,F)+\frac{2\exp(-F)}{F}=\frac{M}{ANl_\rho}, \tag{16}$$

where

$$F(l_\rho,M)\equiv\frac{BN}{E_{\rho\max}}$$

and $\mathrm{Ei}(1,F)=\int_1^\infty t^{-1}\exp(-Ft)dt$ is integral exponent.

B. Isolated head model

Specifying one of M, l_ρ, or $E_{\max}$, Eqs. (16) and (14) allow one to calculate the other two parameters. Figure 11 shows $E_{\max}$ obtained with $M=19$. The model gives a good approximation to the simulated $E_{\max}$ in the steady-state propagation phase. With $M=19$ the width of the space charge layer $l_\rho=0.0156$ cm is in excellent agreement with that defined from 2D calculations (0.0160 cm).

The space charge may be thought of as localized in the equivalent ball of radius l_ρ. The high-field region hence has a radial size of the order of l_ρ. Since emission from the streamer exponentially depends on field, l_ρ represents the

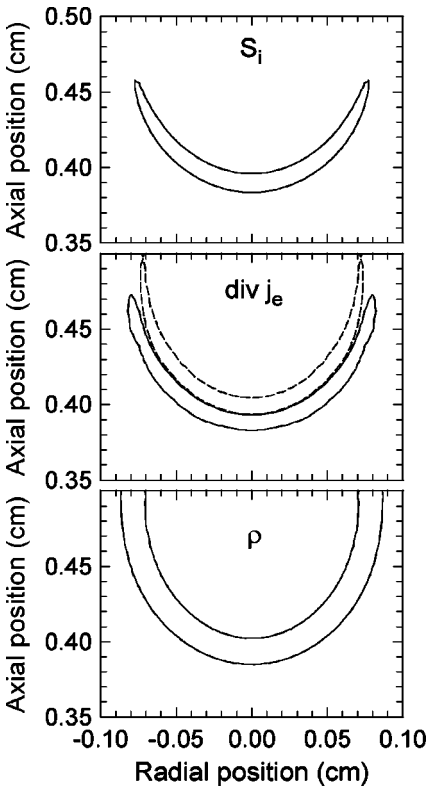

FIG. 7. Contour lines of the rate of ionization S_i, the term $\nabla \cdot \mathbf{j}_e$, and space charge ρ at the moment 17 ns. All the levels corresponds to 0.1 of the maximum value. The dashed curve shows the contour line of the symmetrical negative value of $\nabla \cdot \mathbf{j}_e$. The contour of S_i represents the shape of the ionization domain. The width of the ionization domain is of the order of the width of the space charge layer.

visible radius of the streamer. This radius is 5–6 times less than the radius of the plasma channel (see further discussion). The experimental estimation of the streamer radius in air under similar conditions is within the range 0.002–0.02 cm [29].

In a weak field $E_\rho >> E_L$, and hence at a given M (or l_ρ), the field $E_{\max}$ depends only on the number density of gas molecules, N. According to [19] the electron density in the head,

$$n_h = \frac{\nu_{\max}}{e\mu_e/\varepsilon_0}, \tag{17}$$

is uniquely determined by $E_{\max}$. Here $\nu_{\max} = \mu_e E_{\max} \alpha(E_{\max})$ is the ionization frequency in the field $E_{\max}$. With $E_{\max} \simeq 110$ kV cm^{-1} (Sec. II B), Eq. (17) gives $n_h \simeq 5 \times 10^{13}$ cm^{-3}; the simulation gives $n_h \simeq (2-3) \times 10^{13}$ cm^{-3} [Fig. 3(a)].

In other words within the scope of this model, under a given density of gas molecules streamer dynamics is governed by a single parameter. Any one of M, l_ρ, or $E_{\max}$ can serve as this parameter. This model ignores the existence of the streamer channel; that is why it will be referred to as the isolated head model (IHM).

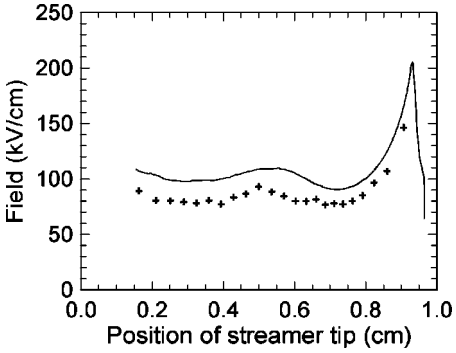

FIG. 8. Peak field $E_{\max}$ at the tip of the streamer (solid curve) and the field of the equivalent ball, Eq. (8) (points) for various positions of the streamer tip.

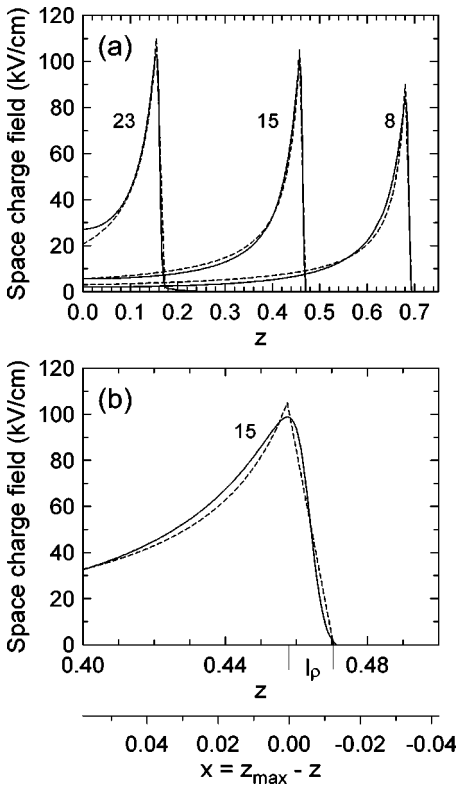

FIG. 9. (a) Solid lines: axial profiles of the space charge field $E_\rho \equiv E - E_L$ from 2D simulations. Dashed lines: the fit (9). The time (ns) is indicated to the left of the curves. (b) Detailed picture for the moment 15 ns. The distance x is counted from the current position $z_{\max}$ of the peak field. The characteristic space scale of fit (9) is l_ρ.

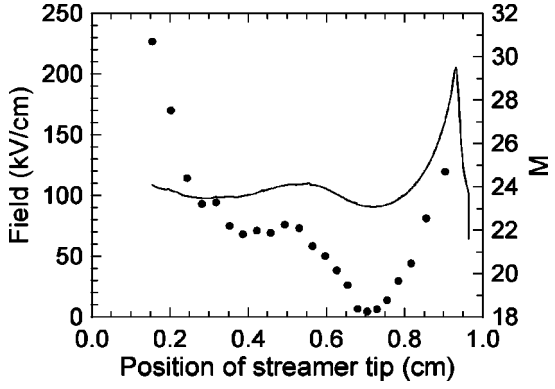

FIG. 10. The field at the tip $E_{\max}$ (solid curve) and ionization integral M, Eq. (10) (points).

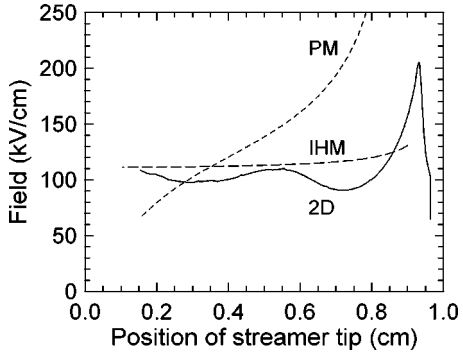

FIG. 11. The field $E_{\max}$ in the gap from 2D simulations (solid line), isolated head model (long dashed line), and potential model (short dashed line).

C. Potential model

The balance of the potential along the streamer axis gives an additional relation between parameters and a potential model (PM) can be formulated. We introduce the space charge voltage drop

$$V_\rho(z_{\max}) \equiv \int_{-l_\rho}^{z_{\max}} E_\rho dx = V_0 - V_L(z_{\max}) - V_c(z_{\max}), \tag{18}$$

where V_c is the voltage drop along the streamer channel and $V_L(z_{\max})=\int_0^{z_{\max}} E_L(x)dx$ is the Laplacian voltage at the tip of the streamer. Figure 12 illustrates V_ρ.

With the fit (9) Eq. (18) gives

$$E_{\rho\,\max} = \frac{2V_\rho}{l_\rho}\left[1+4\ln\left(1+\frac{z_{\max}}{2l_\rho}\right)\right]^{-1}. \tag{19}$$

Equating Eqs. (14) and (19), M is expressed in terms of l_ρ and V_ρ,

$$M = \ln\left\{\frac{8\pi l_\rho V_\rho}{e/\varepsilon_0}\left[1+4\ln\left(1+\frac{z_{\max}}{2l_\rho}\right)\right]^{-1}\right\},$$

and now Eq. (16) gives l_ρ if one specifies V_c. Therefore, within the scope of this model the streamer properties are governed by the voltage drop along the streamer channel V_c.

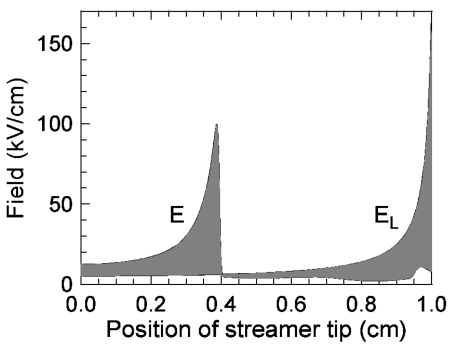

FIG. 12. Axial profiles of the Laplacian field E_L and of the total field E at the moment 17 ns. The space charge voltage drop V_ρ is the shaded area below the curve E. This area equals the shaded area below the curve E_L.

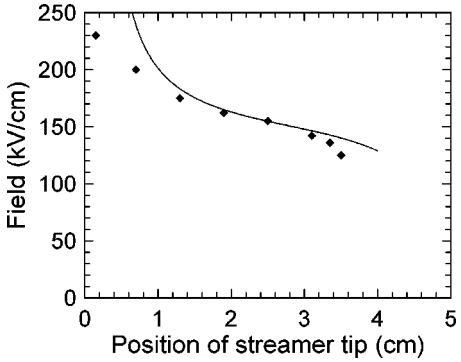

FIG. 13. Peak field $E_{\max}$ of the streamer in a 5-cm point-to-plane gap in air under 20 kV applied voltage. Points: Morrow and Lowke [15] (1.5D model). Solid curve: potential model with $E_c = 2$ kV cm^{-1}. The anode is placed at $z=0$.

The 2D simulation gave a mean field in the streamer channel $E_c \simeq 3$ kV cm^{-1}. The $E_{\max}$ obtained from the PM with $V_c=(d-z_{\max})E_c$ is shown in Fig. 11. As is seen, the $E_{\max}$ is essentially overestimated near the anode.

The first reason for this is that we neglected the Laplacian component of the total field in Eq. (16). Near the anode E_L is large and hence both the IHM and PM are not valid. The second reason is that fit (9) is approximate and does not provide the required value of V_ρ. Far from the tip the field (9) decreases too slowly and the integral over Eq. (9) overestimates the real space charge voltage. In short gaps V_ρ can significantly exceed V_L and the defect in V_ρ can be essential. In longer gaps, when the streamer head is far from the electrodes, $V_\rho < V_L$ and one may expect better results.

It is not easy to compare the PM with experiment, since there are no direct measurements of $E_{\max}$ in streamers. To check the PM in longer gaps the predictions of this model were compared with the 1.5D simulation available in the literature. Figure 13 shows the comparison of $E_{\max}$, calculated by Morrow and Lowke [15] within the scope of the 1.5D model with that predicted by the PM. The applied voltage is 20 kV; the gap spacing is 5 cm. The mean field in the streamer channel was taken to be 2 kV cm^{-1}. As is seen, with this E_c, the results from the PM are very close to those of Morrow and Lowke. The difference is that the PM allows the streamer to propagate towards the cathode, whereas the 1.5D model limits the streamer length by $\simeq 3.6$ cm.

D. Radius of the streamer head, streamer velocity, and current

Remarkably, both presented models do not contain the radius of the streamer head, R_h, since it does not affect the process of the AST. The R_h is the radius of the plasma channel above the tip, which is bounded by the space charge layer (Fig. 7).

The 2D simulations show that the R_h usually exceeds l_ρ by 5–6 times. The radius of the plasma channel is established to transport the current, generated at the tip, to the anode.

To show this we will integrate the space charge continuity equation (7) over the volume shown in Fig. 14. Applying Gauss' theorem, one obtains

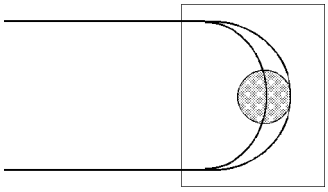

FIG. 14. Sketch of the streamer (Sec. III D): streamer channel, equivalent ball (shaded), and the volume of integration (thin rectangle). The conductivity current flows through the streamer channel. Inside the volume of integration, the charged ball during the time interval τ_ρ, Eq. (21), covers the distance, equal to its radius l_ρ, and this gives the velocity and displacement current.

$$\frac{\partial N_\rho}{\partial t} = j_h \pi R_h^2, \tag{20}$$

since the conductivity current of the density j_h flows mainly in the plasma of the head. The total space charge inside the volume of integration is a charge of the equivalent ball, $N_\rho = \exp(M)$. The time derivative can be approximated as $\partial N_\rho / \partial t \simeq N_\rho / \tau_\rho$, where

$$\tau_\rho = \frac{1}{\nu_{\max}} \ln\left(\frac{n_h}{n_{id}}\right) \tag{21}$$

is a characteristic time of the streamer advancement over the distance l_ρ [9,19]. Here n_{id} is the electron number density on the outside of the ionization domain. The streamer velocity is therefore

$$V_s = \frac{l_\rho}{\tau_\rho} = \frac{l_\rho \nu_{\max}}{\ln(n_h/n_{id})}. \tag{22}$$

Substituting Eq. (21) into Eq. (20) and taking into account that $j_h = \mu_e E_h n_h$, where E_h is the field in the plasma above the tip, one obtains the radius of the head,

$$R_h = \sqrt{\frac{e}{\varepsilon_0} \frac{\exp(M)}{\pi E_h \ln(n_h/n_{id})}}. \tag{23}$$

The R_h weakly depends on the ratio n_h/n_{id}. The logarithm of this ratio usually varies in the range 4–6; a reasonable estimate is $\ln(n_h/n_{id}) \simeq 5$. With $M = 19$ (numerical example in Sec. III B) and $E_h = 3$ kV cm^{-1} the relation (23) gives $R_h = 0.083$ cm. With the same E_h, the potential model gives, at $z = 0.65$, $R_h = 0.082$ cm. Both values are 5 times more than l_ρ (0.016 cm) and agree well with the result of 2D simulations (Fig. 2).

The PM predicts rather an unexpected feature of streamer dynamics: with the growth of the applied voltage the peak field at the tip of the streamer diminishes. Figure 15 shows the results obtained for the conditions of Morrow and Lowke [15] under applied voltages of 20, 30, and 40 kV ($E_c = 2$ kV cm^{-1} in all cases). With the growth of V_0, the space charge width and the head radius increase and $E_{\max}$ diminishes. The decrease of $E_{\max}$ leads to a decrease of the mean electron energy; this can be essential for plasma chemical applications.

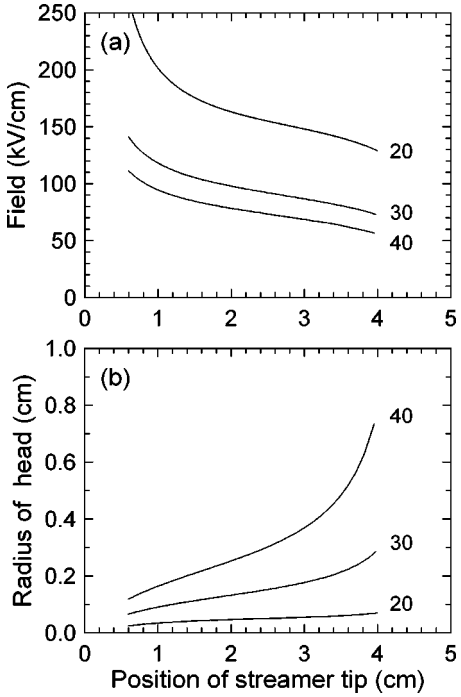

FIG. 15. Streamer parameters in a 5-cm point-to-plane gap in air under applied voltages of 20, 30, and 40 kV (potential model). Conditions of discharge are those of Morrow and Lowke [15]. (a) Peak field $E_{\max}$ at the tip of the streamer, (b) the radius of the streamer head R_h for the same voltages.

Equation (20) allows one to obtain a useful expression for the current in the streamer channel, $I = e\partial N_\rho / \partial t \simeq e N_\rho / \tau_\rho$. Taking into account Eq. (21), one obtains

$$I = \frac{e \exp(M) \nu_{\max}}{\ln(n_h/n_{id})}. \tag{24}$$

This formula can be useful for practical purposes: the current I can be measured in experiment and Eq. (24) gives the relation of $E_{\max}$ and $\exp(M)$. Then the IHM can be applied for the calculation of the other streamer parameters.

IV. DISCUSSION

The Meek's condition of the AST, Eq. (11), does not contain the internal scale of the avalanche. To calculate the field at the tip of an avalanche, Meek [28] used the diffusion radius as an estimate of avalanche size. At the moment of the AST this internal scale arises: it is the width of the space charge layer l_ρ.

Further propagation of the streamer head may be thought of as the movement of a region of the avalanche-to-streamer transition. The ionization domain of the width $\simeq l_\rho$ around the head is a site of the AST. This domain is steady state in the reference frame moving with the head. The charges produced here ''push out'' the electric field towards the cathode, thus providing streamer advancement. The field $E_{\max}$ plays the role of an external field. Unlike the classical AST in a uniform external field, the velocity of the avalanche is a sum of electron drift and streamer velocity. It should be emphasized that the radius of the plasma channel does not affect the

process of the AST and hence has no effect on streamer dynamics.

Within the ID, the rate of photoionization is negligibly small (Fig. 5). Nevertheless, in both the IHM and PM it is assumed that there are a number of seed electrons ahead of the streamer. Simulations show that without photoionization the streamer does not propagate. However, the exact number of seed electrons ahead of the tip is not essential: it affects the value of n_{id}, which appears in all formulas under the sign of a logarithm. In a weak field the role of photoionization is to provide at least one seed electron ahead of the tip. Further multiplication of charges occurs due to collisional ionization.

Figure 5 shows that diffusion plays no part in streamer advancement.

The PM predicts streamer expansion under a high applied voltage. Streamers with a head radius of about 1 cm were detected in [30]. The experiments were made in air between coaxial wire and a tube of radius 15 cm under an applied voltage of $\sim$100 kV. Photographs clearly show bright plasma balls with a radius of about 1 cm in the middle of the gap. The external field at this point is below 30 kV cm^{-1}. The effect can be attributed to the growth of the space charge voltage drop V_ρ, as described above.

Both the IHM and PM use the fit (9). In air this fit was found to be valid for various applied voltages and anode geometries. However, we did not make attempts to check the validity of relation (9) for other gases. The potential model can be improved by using more sophisticated approximations for the space charge field instead of Eq. (9). At a large distance from the tip E_ρ should decrease faster than $1/x$.

The use of the space charge field E_ρ instead of the total field $E=E_\rho+E_L$ in the expression for α, Eq. (5), gives the relatively simple equation (16). An attempt to account for the Laplacian field in Eq. (5) leads to cumbersome expressions, which involve the specific geometry of electrodes. However, one may expect that near the electrodes, where E_L is large, this approach would give more accurate results.

ACKNOWLEDGMENTS

Two-dimensional calculations have been performed on the mainframe computer of Eindhoven University of Technology (The Netherlands) via the Internet. The author is grateful to Dr. Eddie van Veldhuizen and to Professor W. Rutgers for their interest in this work. The author is also grateful to Dr. P. P. M. Blom from EUT for the excellent pictures of streamer corona in air under high voltages.

[1] W. Rogowski, Arch. Elektrotech. **20**, 99 (1928).
[2] *Non-Thermal Plasma Techniques for Pollution Control*, Vol. 34A of *NATO Advanced Study Institute, Series G*, edited by B. M. Penetrante and E. Shultheis (Springer, Berlin, 1993).
[3] S. Dhali and P. F. Williams, J. Appl. Phys. **62**, 4696 (1987).
[4] C. Wu and E. E. Kunhardt, Phys. Rev. A **37**, 4396 (1988).
[5] E. E. Kunhardt and Y. Tzeng, Phys. Rev. A **38**, 1410 (1988).
[6] J.-M. Guo and C.-H. Wu, *Comparisons of Multidimensional Fluid Models for Streamers*, Vol. 34A of *NATO Advanced Study Institute, Series G*, edited by B. M. Penetrante and E. Shultheis (Springer, Berlin, 1993), pp. 287–298. See Ref. [2].
[7] P. A. Vitello, B. M. Penetrante, and J. N. Bardsley, Phys. Rev. E **49**, 5574 (1994).
[8] A. A. Kulikovsky, J. Phys. D **28**, 2483 (1995).
[9] A. A. Kulikovsky, J. Phys. D **30**, 441 (1997).
[10] A. J. Davies and C. J. Evans, Proc. IEEE **114**, 1547 (1967).
[11] P. Bayle and B. Cornebois, Phys. Rev. A **31**, 1046 (1985).
[12] R. Morrow, Phys. Rev. A **35**, 1778 (1987).
[13] N. L. Aleksandrov and E. M. Bazelyan, J. Phys. D **29**, 740 (1996).
[14] F. Grange, N. Soulem, J. F. Loiseau, and N. Spyrou, J. Phys. D **28**, 1619 (1995).
[15] R. Morrow and J. J. Lowke, J. Phys. D **30**, 614 (1997).
[16] J. M. Guo and J. Wu, IEEE Trans. Plasma Sci. **24**, 1348 (1996).
[17] G. A. Dawson and W. P. Winn, Z. Phys. **183**, 159 (1965).
[18] I. Gallimberti, J. Phys. D **5**, 2179 (1972).
[19] I. M. Dyakonov and V. Y. Kachorovskii, Zh. Éksp. Teor. Fiz. **94**, 321 (1988) [Sov. Phys. JETP **67**, 1049 (1988)].
[20] L. B. Loeb, Science **148**, 1417 (1965).
[21] M. C. Wang and E. E. Kunhardt, Phys. Rev. A **42**, 2366 (1990).
[22] Y. P. Raizer and A. N. Simakov, Fiz. Plasmy **22**, 668 (1996).
[23] R. S. Sigmond, J. Appl. Phys. **56**, 1355 (1984).
[24] J. W. Gallaher, E. C. Beaty, J. Dutton, and L. C. Pitchford, J. Phys. Chem. Ref. Data **12**, 109 (1983).
[25] M. B. Zheleznyak, A. K. Mnatsakanian, and S. V. Sizykh, Teplofiz. Vys. Temp. **20**, 423 (1982).
[26] A. A. Kulikovsky, J. Comput. Phys. **119**, 149 (1995).
[27] Y. Creyghton, B. Smeets, E. M. van Veldhuizen, and W. R. Rutgers, in *Proceedings of the International Conference on Gas Discharges and Their Applications*, edited by D. W. T. Williams (University College of Swansea, Swansea, UK, 1992).
[28] J. M. Meek, Phys. Rev. **57**, 722 (1940).
[29] A. Gilbert and F. Bastien, J. Phys. D **22**, 1078 (1989).
[30] P. P. M. Blom, Ph. D. thesis, Eindhoven University of Technology, 1996.